

Combined time and frequency spectroscopy with engineered dual-comb spectrometer

Sutapa Ghosh¹* and Gadi Eisenstein

Andrew and Erna Viterby Department of Electrical Engineering and Russell Berrie Nanotechnology Institute, Technion-Israel Institute of Technology, Haifa 32000, Israel

 (Received 1 April 2023; revised 17 June 2023; accepted 7 August 2023; published 5 September 2023)

Dual-comb spectroscopy (DCS) is a powerful technique for broadband spectroscopy with high precision. High-frequency resolution requires long data acquisition times, limiting the temporal resolution in time-resolved measurements. We overcome this limitation by engineering the interaction between the sample under test and the DCS pulsed laser. The DCS interferogram is measured in steps with every step comprising a different number of pulses that interact with the sample. The sample's complex properties (absorption and phase) are extracted from the Fourier transform of the interferogram as a function of the number of pulses; this maps the temporal evolution of the excited state population. A two-dimensional spectrum is generated from which the system time evolution is deduced. We benchmark this method by measuring the two-dimensional spectrum of a room-temperature rubidium vapor. The measured population dynamics of the excited state show a square dependence on the number of interacting pulses due to the coherent accumulation of population. Rabi oscillations are observed under intense excitation conditions. This is the first demonstration of DCS with high frequency and high temporal resolutions (which is given by the inverse of the repetition rate of the comb laser) without invoking pump-probe spectroscopy, combining the pulsed laser spectral and temporal properties. This method allows one to detect simultaneously the kinetics of different chemical species and hence the pathway for chemical reactions.

DOI: [10.1103/PhysRevResearch.5.033158](https://doi.org/10.1103/PhysRevResearch.5.033158)

I. INTRODUCTION

Dual-comb spectroscopy (DCS) is a powerful broadband method offering high resolution, fast acquisition times, and mechanical stability as no moving part is involved [1,2]. DCS developed hand in hand with advancements in ultrashort-pulse technology and laser stabilization methods. When a comb laser passes through the sample, the complex properties of the sample are imprinted on the laser spectrum. After beating with the second laser, these characteristics are retrieved in the RF domain. Since its first demonstration [3–5], the DCS method has been used to characterize a large variety of chemical species [6–10].

DCS uses two pulsed lasers to probe and measure the spectrogram of a sample. Depending on the desired frequency resolution, the DCS interferogram needs to be measured for a certain acquisition time. This limits the possible time resolution of the DCS method to study time-resolved events. The dynamical properties of the probed sample are difficult to extract due to the long data acquisition times needed for high spectral resolutions and signal-to-noise ratio (SNR) [1,11,12].

Recently, there have been considerable efforts to combine the time aspects of the pulsed laser in the DCS method to per-

form time-resolved measurements [13–15]. However, the time resolution using conventional DCS has been limited to the μs time range. A DCS system combined with an amplitude-modulated CW laser was used to perform time-resolved measurement with a time resolution of 100 μs , measuring a spectral span of 36 GHz with a frequency resolution of 100 MHz [16]. Here, the change in the absorption spectrum of the P(27) line of the $\nu_1 + \nu_3$ band in acetylene was measured as a function of an increase in the gas pressure. In another experiment, the time-resolved DCS method showed simultaneous production of C_2H_6 and the vibrational excitation of CH_4 molecules in a CH_4/He gas mixture, in the presence of an electric discharge with a time resolution of 20 μs [17]. Various techniques have been introduced to increase the time resolution, such as intracavity optical filtering that increases the comb tooth spacing, which improves the data acquisition speed and the time resolution to 11 μs [18,19]. Burst-mode DCS in which each pulse is multiplexed into a short train of pulses [20] was used to study the transmission spectra of 22 Nd lines. An effective acquisition rate of 25 kHz with 40 μs time resolution was demonstrated.

Conventional DCS, in combination with pump-probe spectroscopy, was shown to attain time resolutions of the order of femtoseconds [21,22], set by the delay between the pump and the signal laser, which is controlled by moving a mirror pair on a mechanical translation stage which reduces the mechanical stability of the system. Also, its slow motion affects the data acquisition speed, which eliminates the unique advantages of DCS. An alternative approach to replace the translation stage in pump-probe DCS spectroscopy has been reported where another comb with a slightly different repetition rate

*Corresponding author: sutapa.g@campus.technion.ac.il

Published by the American Physical Society under the terms of the Creative Commons Attribution 4.0 International license. Further distribution of this work must maintain attribution to the author(s) and the published article's title, journal citation, and DOI.

compared to the pump comb was used [23]. This automatically scans the signal laser in time and later combines with the reference laser to generate the DCS spectrum. The data acquisition speed and stability are preserved at the cost of the complexity involved in using three stabilized comb lasers and an additional CW laser, to compensate for both the path length and the offset frequency fluctuations.

DCS with transient absorption also allows pump-probe spectroscopy without using mechanical stages and with high temporal resolution (fs to ns) [24]. This method is limited however to materials whose transient decay time is faster than the repetition rate of the laser. Also, since the transient population decay is measured in the time domain, it is difficult to extract a frequency response in order to discriminate between responses representing different transitions or those originating from a mixture of gases that are excited simultaneously by broadband comb lasers.

In this paper, we propose and demonstrate a modulated dual-comb spectroscopy technique where engineering the interaction between the sample and the probe laser enables high temporal resolutions. In this method, multiple DCS interferograms are measured, each time with a different number of pulses probing the sample in a single interferogram. This allows one to measure a two-dimensional spectrum with one axis representing frequency, as in conventional DCS, with the second axis describing the sample characteristic as a function of the number of pulses interacting with the sample, which directly translates into a time response of the sample probing at the repetition rate. This method allows time-resolved measurement with the resolution given by the inverse of the repetition rate of the laser while simultaneously measuring the broadband spectrum.

We use the modulated DCS method to measure the multidimensional DCS spectrum of room-temperature rubidium atoms. The population dynamics of the excited state of various hyperfine transitions of rubidium isotopes were observed. The population initially grows as the square of the number of interacting pulses and then exhibits Rabi oscillations. The quadratic transient arises from the coherent accumulation of the population of the rubidium atoms interacting with the pulse train. The Rabi oscillations are due to the strong excitation. We measured a spectral span of 25 GHz with a frequency resolution of 250 MHz, and the population evolution was measured with a temporal resolution of 4 ns.

II. PRINCIPLE OF MODULATED DUAL-COMB SPECTROSCOPY

The maximum frequency resolution of the DCS spectrometer is given by the repetition rate of the laser probing the sample. The basic principle behind the conventional DCS method is shown in Fig. 1(a). Two combs with slightly different repetition rates are used, and an interferogram is measured where the length of each interferogram is given by the inverse of the difference between the repetition rate of the two lasers ($1/\delta f_{\text{rep}}$). This limits the time resolution of the time-resolved measurement of the sample properties to $1/\delta f_{\text{rep}}$. The value of δf_{rep} is determined by the total optical spectrum that needs to be measured and the signal-to-noise ratio (SNR) which is defined as the ratio between the signal peak-to-peak strength

to the background noise. This limits the resolution of time-resolved DCS measurement to a few microseconds.

The technique we propose and demonstrate lifts the limitation on the time resolution of DCS measurements by engineering the interaction between the sample under test and the pulse train. The laser pulse train is amplitude modulated with a rectangular pulse whose width determines the number of short pulses that interact with the sample, as shown in Fig. 1(b). The repetition rate of the modulated signal is chosen such that the sample fully relaxes between two consecutive modulation cycles. This makes the measured dynamic response repetitive with each modulation cycle, which is then sampled by the reference laser and detected on a photodetector, as shown in Fig. 1(c). In each consecutive cycle, the modulation pulse widens, allowing more pulses to interact with the sample. Repeating these sequences leads to the extraction of the sample properties as a function of the number of (the temporally separated) probe pulses. The averaged sample dynamic response is extracted with a time resolution given by the probing time, $1/f_{\text{rep}}$. A two-dimensional spectrum is generated by combining the frequency and time dependencies of the sample properties shown in Fig. 1(c).

The electric field of the probe laser pulse train in the Fourier domain is given by

$$E_p(f) = \frac{1}{T_{\text{rep}}} \sum_l \mathcal{F}[E_p(t)](f) \delta(f - lf_{\text{rep}}), \quad (1)$$

where $\mathcal{F}[E_p(t)](f)$ represents the Fourier transform of an envelope $E_p(t)$. This represents the optical spectrum with discrete frequency lines separated by the repetition rate of the laser, $f_{\text{rep}} = 1/T_{\text{rep}}$. After the modulation, the electric field becomes $E_{\text{mod}}(t) = y(w, t)E_p(t)$, where $y(w, t)$ is the modulating signal. We use a rectangular modulation signal with width, w , which acts like a filter controlling the number of probe pulses. The Fourier transform of the modulated pulse train is

$$E_{\text{mod}}(f) = \frac{1}{2\pi T_{\text{rep}} T} \sum_l \sum_m \mathcal{F}[y_0](f - lf_{\text{rep}}) \mathcal{F}[E_p] \times (lf_{\text{rep}}) \delta\left(f - lf_{\text{rep}} - \frac{m}{T}\right). \quad (2)$$

The period of the modulation signal, T , is chosen to be longer than the atomic relaxation time and shorter than the pulse train repetition rate, and $\mathcal{F}[y_0]$ are the Fourier transform of $y(w, t)$. l and m are integers representing the frequency components of the pulse train and the sidebands due to the modulation. This equation calculates the Fourier domain spectrum for different modulation widths. The detailed calculation is presented in Sec. I of the Supplemental Material [25].

The repetition rate of the modulation signal is a fraction of that of the probe laser; in the present case it is 25 MHz. In the frequency domain, the intensity modulation adds sidebands to the carrier modes at f_{rep} with a periodicity of 25 MHz. As the number of pulses in one modulation cycle increases, the intensity of the sidebands decreases, transferring more optical power to the carrier frequency. This preserves the sampling of the probe laser spectrum by the reference laser as shown in Fig. 1(b) (bottom figure). As the absorption spectrum is measured with different widths of the modulation signal, the

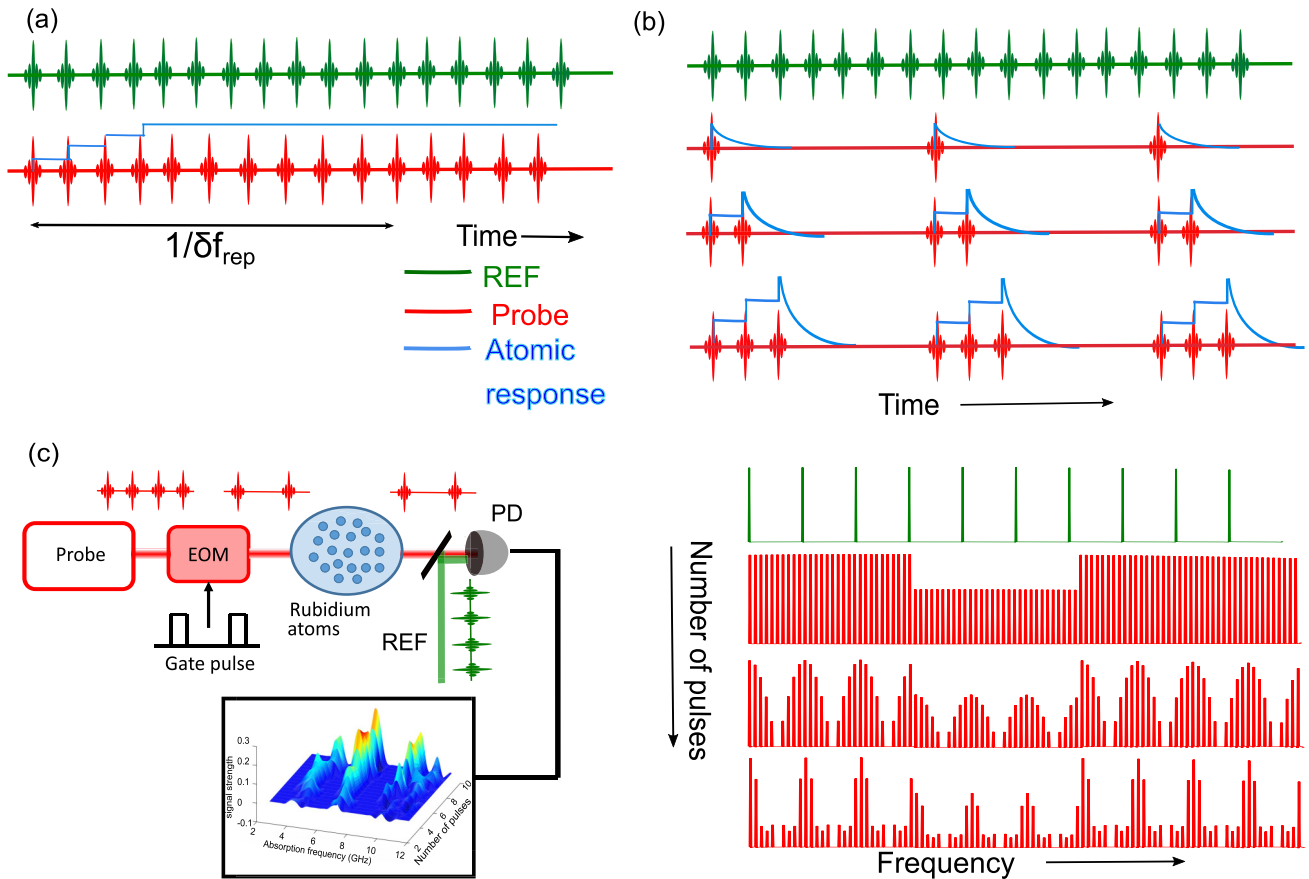


FIG. 1. Principle of modulated dual-comb spectroscopy (DCS). (a) The conventional DCS method requires measurements of many probe (red) pulses for a single interferogram of length $1/\delta f_{\text{rep}}$ limiting the time resolution of the method. The DCS spectrum is obtained by mixing the probe laser with a reference laser, REF (green), that contains the sample response (blue) at steady state. (b) The modulated DCS method measures the dynamic response of the sample induced with each probe pulse by performing a series of measurement each using a different number of probe pulses interacting with the sample under test in one interferogram. In the frequency domain, the intensity modulation adds sidebands to the carrier modes at f_{rep} with a periodicity of the modulation frequency. As the number of pulses in one modulation cycle increases the intensity of the sidebands decreases, transferring more optical power to the carrier frequency. The sample response is extracted by measuring the absorption depth as a function of the number of probe pulses. (c) Schematic of the modulated DCS method with a gated intensity modulator, EOM, controlling the number of pulses interacting with the sample. After mixing with the REF laser, a two-dimensional spectrum is generated

data are acquired for times that ensure a sufficient frequency resolution and a high SNR.

As the modulation width increases, the Fourier spectral intensity of the DCS beat spectrum increases linearly with the number of pulses, as shown in Sec. I of the Supplemental Material (Fig. S1) [25]. The sample absorption is measured as a difference between the absorption dip and the background and is unaffected by normalization. To check the validity of our method numerically, we simulated a sample with a quadratic population dependence on time, which we retrieved by calculating the two-dimensional spectroscopy, as shown in the Supplemental Material (Fig. S2) [25].

III. EXPERIMENTAL SETUP

Figure 2 describes an overview of the hybrid dual-comb spectroscopy apparatus. The probe laser is a commercial fiber laser (Menlo Systems, FC1500-250-ULN) with a repetition rate of 250 MHz. The probe laser is RF locked to a GPS signal that provides absolute long-term stability of 2×10^{-12}

at 1 second. The reference laser is an active mode-locked semiconductor laser (MLL) detuned by 25 kHz from the probe laser repetition rate. It employs a piezo-mounted mirror in the cat-eye configuration and an intracavity interference filter. The MLL is injection locked by an external cavity CW laser which is locked, in turn, on a single tooth of the probe laser. The beat between the CW laser and the probe laser is used to stabilize the CW laser by applying a fast feedback to an acousto-optic modulator, AOM2, and a slow feedback to the piezo-mounted cavity mirror. The fully stabilized MLL emits pulses with a duration of 50 ps. A mutual coherence time of 100 seconds was achieved in the present DCS system [26]. Figure 2(b) shows the measured DCS spectrum with marked transitions of the rubidium vapor (Rb-87 and Rb-85). The SNR is plotted in Fig. 2(c) as a function of different integration times. The slope of 0.51 confirms the square root dependence of SNR on the integration time preserving the coherence of the DCS system up to 100 seconds.

The probe laser is amplitude modulated by an electro-optic Mach-Zehnder modulator from EO space which is driven by

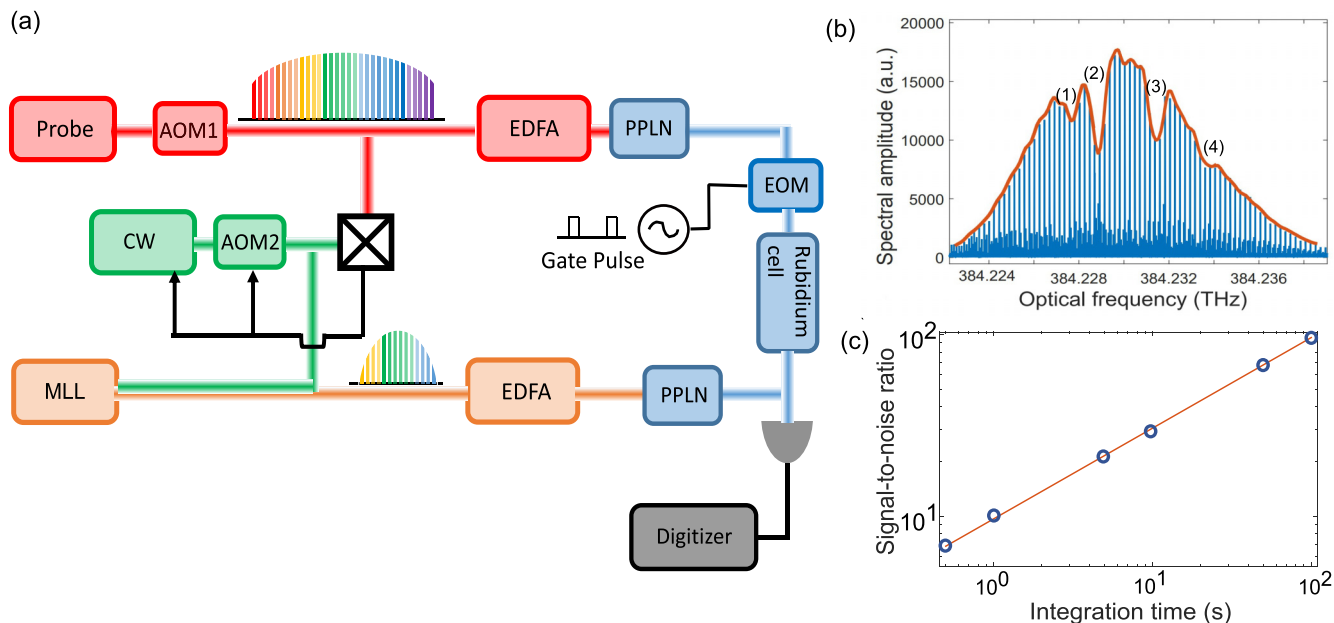


FIG. 2. Schematic of the hybrid setup for dual-comb spectroscopy. (a) Hybrid DCS system comprising a commercial fiber-based frequency comb (probe) and an injection-locked active mode-lock semiconductor laser (REF). Each laser is amplified by an erbium-doped amplifier (EDFA) and frequency-doubled through a periodically poled lithium niobate (PPLN). The probe laser passes through an intensity modulator (EOM) and mixed with the REF laser. It is then measured with the photodetector (PD) and digitized. (b) The Fourier spectrum of the DCS interferogram is shown with 100 seconds of data integration time. Four Doppler-broadened peaks of rubidium mixtures (Rb-85 and Rb-87) are extracted. By the combination of electrical injection locking of the repetition rate of the MLL and optical injection locking by the CW laser, 100 seconds of mutual coherence has been established between the two DCS lasers.

an arbitrary wave-form generator (AWG), Agilent Technologies, 81150A. To modulate probe laser pulses, the modulation signal from the AWG needs to be synchronized to the repetition rate of the probe pulses. To this end, we derived an RF signal of 250 MHz from the probe laser repetition rate and used it as a reference to a phase-locked oscillator that generates a 25 MHz clock signal for the AWG.

Both lasers were tuned to 1560 nm and are amplified by an erbium-doped fiber amplifier (EDFA) before being frequency doubled using temperature-stabilized periodically poled lithium niobate crystals. The frequency-doubled modulated probe pulses pass through a vapor cell filled with rubidium isotopes (^{85}Rb and ^{87}Rb) held at room temperature. After interacting with the gas sample in a single-pass configuration, the two frequency-doubled lasers are mixed and detected by a photodetector, FPD610-FC-VIS. The detected signal is filtered, amplified, and digitized. A fast Fourier transform is computed from the data and the amplitude of the spectrum is retrieved as displayed in Fig. 2(b).

IV. RESULTS

Demonstration of modulated dual-comb spectroscopy. The intensity modulator (EOM) is driven by an AWG that applies a rectangular pulse with a repetition rate of $1/T$ and width w , thereby selecting the number of interacting pulses. The pulses interact with the sample, and by the end of each cycle, the sample relaxes to its ground state so that the sequence is repeated at the repetition rate of the modulation pulse train. The data is recorded for a sufficiently long time to ensure the required spectral resolution. In the present experiment, δf_{rep}

was 25 kHz, meaning that a single interferogram is $1/\delta f_{\text{rep}} = 40 \mu\text{s}$ long. Since the reference laser pulse width is around 50 ps, the number of overlapped pulses was $\Delta t_{\text{width}} f_{\text{rep}}^2 / \delta f_{\text{rep}} = 100$ in each interferogram. For a modulation repetition rate of 25 MHz, the number of overlapping pulses for the minimum modulation width decreases to 10 pulses in each interferogram. The data acquisition time in the current experiment was 50 ms, yielding 1250 averaged and Fourier transformed interferogram. The rubidium DCS spectrum was measured as a function of the number of pulses that interacted with the rubidium atoms.

Multidimensional spectroscopy of rubidium atoms. To demonstrate the method, we study a two-level atom (rubidium vapor) excited by a train of pulses. The Hamiltonian for this system is $H = H_{\text{atom}} + H_{\text{int}}$, where $H_{\text{atom}} = \hbar\omega_0\sigma^{\dagger}\sigma$ and $H_{\text{int}} = \hbar\Omega(\sigma e^{i\omega t} + \sigma^{\dagger} e^{-i\omega t})$, $\sigma = |g\rangle\langle e|$, and Ω is the Rabi frequency defined as $\Omega = -\frac{\langle g|\hat{e}\cdot d|e\rangle E_{\text{mod}}(t)}{\hbar}$; d is the dipole moment of the atom interacting with the modulated pulse train electric field, $E_{\text{mod}}(t)$.

Since the interpulse separation is smaller than the atomic relaxation times, the population of the atoms is coherently accumulated with each pulse. It shows a square dependence on the number of accumulated pulses [27,28]. If the excitation is sufficiently strong, the population transfers periodically between the ground and excited states exhibiting Rabi oscillations [29]. Usually, it is difficult to observe Rabi oscillations in room-temperature atomic ensembles due to the fast atomic decoherence times. Probing the atoms with a high-intensity pulse train drives fast, coherent dynamics in the system, which can then be measured using the modulated DCS method, and

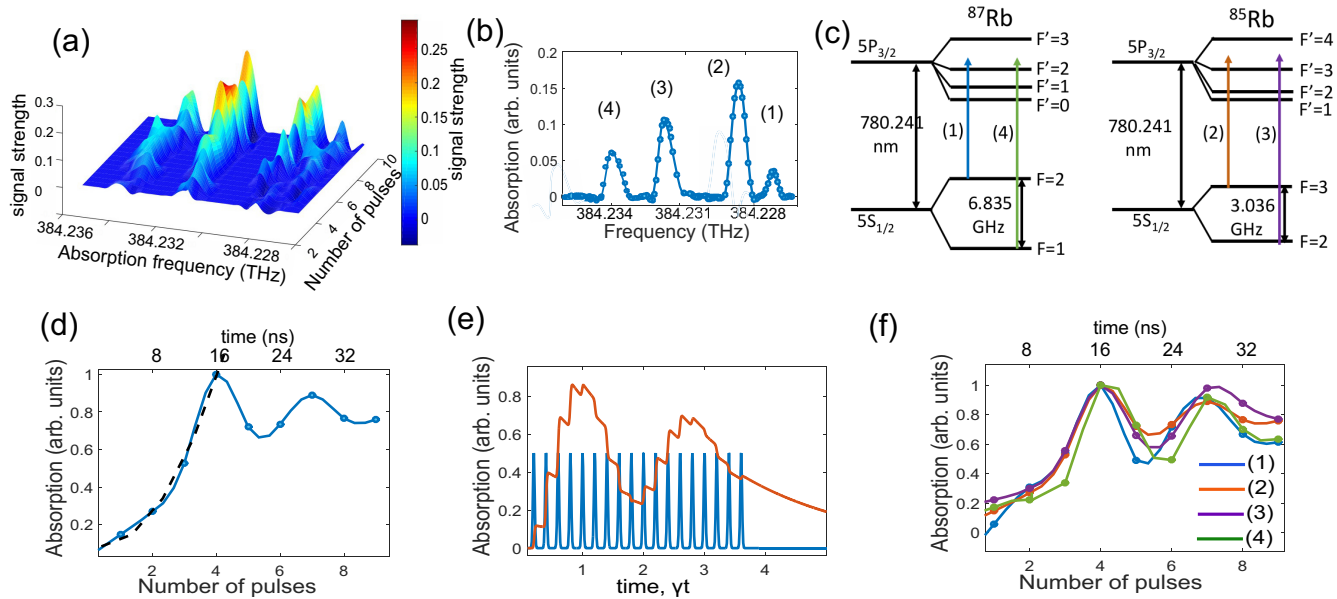


FIG. 3. Two-dimensional dual-comb spectroscopy. (a) Experimental results of the two-dimensional rubidium spectrum as a function of the absorption frequency and the number of temporally separated interacting pulses. (b) The horizontal axis represents the absorption spectrum of the Doppler broadened transitions of the rubidium isotopes marked for the transitions shown in the level diagram in (c). (d) The vertical axes of the two-dimensional spectrum represents the population evolution of the rubidium atoms in the excited state probed with pulses at different times. The population dynamics show a square dependence on the number of accumulated pulses (black dashed) and Rabi oscillation due to the intense excitation. (e) The experimental data are consistent with the simulation results of the population evolution (red) of the two-level system interacting with the pulse train (blue). (f) The temporal evolution of the excited state population corresponds to each transition of the rubidium mixture.

also exhibit Rabi oscillations. The Rabi frequency depends only on the intensity of an individual pulse and not on the accumulated intensity of multiple pulses, since those pulses are not temporally overlapped. The rubidium atoms were probed with different numbers of pulses, each separated by 4 ns. The relaxation time of both rubidium isotopes ^{85}Rb and ^{87}Rb is around 27 ns for the $5P_{3/2}$ state [30–32].

In the experiment, we recorded the absorption spectrum corresponding to various hyperfine transitions. The background-subtracted absorption spectrum as a function of the number of interacting pulses is plotted as a multidimensional spectrum in Fig. 3(a). Figure 3(b) represents the rubidium absorption spectrum corresponding to a specific modulation width with six interacting pulses. The Doppler-broadened transitions are marked according to the level diagram in Fig. 3(c). Figure 3(d) describes the temporal evolution of the population in the excited state of $5S_{1/2}(F=3) \rightarrow 5P_{3/2}$ transition in a ^{85}Rb isotope. The population evolution has a square functional form due to the coherent accumulation of the pulses, while the oscillation represents the Rabi oscillation at $2\pi \times 13.28$ MHz. The optical power of the probe beam is 10 mW, and the spectral width is 6 nm. It is focused to a beam diameter of 500 μm when transversing the Rb sample. This yields a Rabi oscillation of $2\pi \times 12.5$ MHz, which is roughly equivalent to the experimental value (the dipole moment used in the calculation is $4.227ea_0$, where e is the electron charge and a_0 is the Bohr radius). Figure 3(e) shows simulation results of the Bloch equations corresponding to the Hamiltonian for the parameters of the present

experiment, which qualitatively agrees with the data. Figure 3(f) shows the temporal evolution of all the marked transitions. Since the dipole moments of both the rubidium isotopes for the transition $5S_{1/2} \rightarrow 5P_{3/2}$ are the same, they exhibit Rabi oscillations with the same frequency [31,32]. The numerical simulation to calculate the population dynamics of atoms has been performed with a “quantum optics toolbox” in Julia [33], with modifications to introduce the effect of the pulse train.

Optimization of modulation parameters. The theory assumes that the atoms relax completely to the ground state between the modulation cycles. As the modulation pulse width increases, the temporal separation between consecutive modulation cycles may become insufficient for the atoms to relax completely. In this case, the population transfer still shows similar features, but the strength of the population transfer is reduced. Figure 4(a) describes a simulation of the temporal behavior of the excited state as a function of a number of pulses, N . Figures 4(b) and 4(c) show the excited state population for $N = 20$ and $N = 5$. For $N = 5$, the atoms relax completely, and the signal strength recovers in every modulation cycle. For $N = 20$, the atoms do not relax completely, so the population transfer to the excited state decreases in each consecutive cycle and eventually attains some equilibrium level. The population evolution profile is still preserved, but the signal strength decreases. This problem can be solved by increasing the modulation period so that atoms relax to the ground state completely, as shown in Fig. 4(d), where the excited state population is plotted as a function of T , the

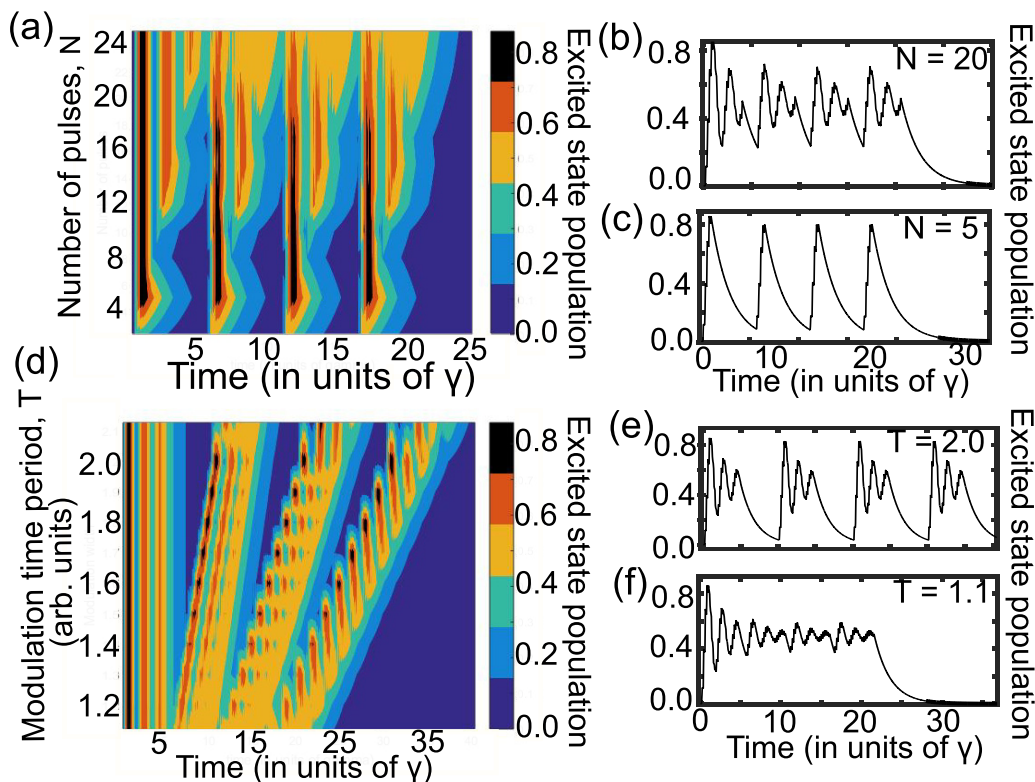


FIG. 4. Simulated dependence of the excited state population on the modulation signal parameters. (a) Excited state population is shown as a function of the number of pulses interacting with the atoms in each modulation cycle. The horizontal axis represents time normalized by the system decoherence time, γ . (b) and (c) represent the population transfer for a number of pulses in each cycle, $N = 20$ and $N = 5$, respectively. For a fixed modulation width, as the number of pulses in each modulation cycle increases, an atom does not relax completely to the ground state, which changes the population dynamics at different cycles. In general, the shape of the population transfer is preserved, and the DCS measurement will record the averaged evolution profile. (d) The population of the excited state as a function of the different modulation periods (T) and the evolution time (t/γ) is shown. (e) Population transfer for $T = 2.0$ shows identical population dynamics with each modulation cycle in contrast to the case (f) $T = 1.1$ when the atom does not relax completely, and the population transfer decay with time.

modulation cycle. Figures 4(e) and 4(f) show the population evolution for $T = 1.1$ and $T = 2.0$. The atoms are not relaxed to the ground state for the short cycle, so the population transfer differs between modulation cycles, in contrast to the long cycles, where the signal strength is recovered. The modulation period determines the dynamic range that can be measured for a system with a given decoherence time, γ . For the large values of γ , the population decays rapidly to the ground state, and shorter modulation periods can be used.

V. DISCUSSION

We introduced a new DCS scheme that allows high temporal resolution by engineering the interaction between the laser pulse train and the sample. As proof of concept, we applied this method to a mixture of rubidium isotopes. We demonstrate that the technique enables broadband spectroscopy with the frequency resolution given by the repetition rate of the probe laser, separating the various hyperfine transitions of the Doppler-broadened rubidium isotopes. Also, it measures the population evolution into the excited state with a time resolution given by the inverse of the repetition rate of the laser. Our measurement also shows Rabi oscillations imprinted on the population dynamics.

The time resolution of the modulated DCS method depends on the laser repetition rate, with high repetition rate allowing measuring fast processes. In the present setup, the temporal resolution is 4 ns. It is possible of course to use very high repetition rates. An extreme example is a chip scale comb with a repetition rate of 450 GHz [34] that offers a time accuracy of 2.22 ps, limiting the frequency resolution to 450 GHz. However, the relevant transition can still be excited by scanning the comb laser frequency around the molecular excitation frequency by tuning the repetition rate.

Combining the time and frequency aspects of a pulsed laser in DCS makes it a powerful spectroscopic tool. This type of spectroscopy is especially beneficial for studying complicated chemical reactions that lead to many metastable and short-lived chemical compounds produced during the reaction [17]. Due to the broadband nature, most chemical species are likely to be detected. At the same time, the temporal aspects can extract information about the path of the chemical reaction from the parent compound mixture to the final product mixture. The technique we propose can be used for spectroscopic examinations of almost every material provided that the dynamics are smaller than the measurement resolution, which can be increased by operating with high-repetition-rate mode-locked lasers. Examples include III-V semiconductors

such as multiple quantum wells and quantum dots in the GaAs and InP family of compounds [35]. Other applications of the

technique include measurement of electron spin relaxation [36] or coherence time of nonradiative excitons [37].

-
- [1] I. Coddington, N. Newbury, and W. Swann, Dual-comb spectroscopy, *Optica* **3**, 414 (2016).
- [2] N. Picqué and T. W. Hänsch, Frequency comb spectroscopy, *Nat. Photonics* **13**, 146 (2019).
- [3] F. Keilmann, C. Gohle, and R. Holzwarth, Time-domain mid-infrared frequency-comb spectrometer, *Opt. Lett.* **29**, 1542 (2004).
- [4] M. Brehm, A. Schliesser, and F. Keilmann, Spectroscopic near-field microscopy using frequency combs in the mid-infrared, *Opt. Express* **14**, 11222 (2006).
- [5] T. Yasui, E. Saneyoshi, and T. Araki, Asynchronous optical sampling terahertz time-domain spectroscopy for ultrahigh spectral resolution and rapid data acquisition, *Appl. Phys. Lett.* **87**, 061101 (2005).
- [6] E. Baumann, F. R. Giorgetta, W. C. Swann, A. M. Zolot, I. Coddington, and N. R. Newbury, Spectroscopy of the methane ν_3 band with an accurate midinfrared coherent dual-comb spectrometer, *Phys. Rev. A* **84**, 062513 (2011).
- [7] A. Zolot, F. Giorgetta, E. Baumann, W. Swann, I. Coddington, and N. Newbury, Broad-band frequency references in the near-infrared: Accurate dual comb spectroscopy of methane and acetylene, *J. Quant. Spectrosc. Radiat. Transfer* **118**, 26 (2013).
- [8] G. B. Rieker, F. R. Giorgetta, W. C. Swann, J. Kofler, A. M. Zolot, L. C. Sinclair, E. Baumann, C. Cromer, G. Petron, C. Sweeney, P. P. Tans, I. Coddington, and N. R. Newbury, Frequency-comb-based remote sensing of greenhouse gases over kilometer air paths, *Optica* **1**, 290 (2014).
- [9] M. B. Sajid, E. Es-sebbar, T. Javed, C. Fittschen, and A. Farooq, Measurement of the rate of hydrogen peroxide thermal decomposition in a shock tube using quantum cascade laser absorption near 7.7 μm , *Int. J. Chem. Kinet.* **46**, 275 (2014).
- [10] R. Spearrin, S. Li, D. Davidson, J. Jeffries, and R. Hanson, High-temperature iso-butene absorption diagnostic for shock tube kinetics using a pulsed quantum cascade laser near 11.3 μm , *Proc. Combust. Inst.* **35**, 3645 (2015).
- [11] N. R. Newbury, I. Coddington, and W. Swann, Sensitivity of coherent dual-comb spectroscopy, *Opt. Express* **18**, 7929 (2010).
- [12] A. Nishiyama, S. Yoshida, T. Hariki, Y. Nakajima, and K. Minoshima, Sensitivity improvement of dual-comb spectroscopy using mode-filtering technique, *Opt. Express* **25**, 31730 (2017).
- [13] M. A. Abbas, Q. Pan, J. Mandon, S. M. Cristescu, F. J. M. Harren, and A. Khodabakhsh, Time-resolved mid-infrared dual-comb spectroscopy, *Sci. Rep.* **9**, 17247 (2019).
- [14] P.-L. Luo and I.-Y. Chen, Synchronized two-color time-resolved dual-comb spectroscopy for quantitative detection of HO_x radicals formed from Criegee intermediates, *Anal. Chem.* **94**, 5752 (2022).
- [15] S. Ghosh and G. Eisenstein, Fast High-Resolution Measurement of an Arbitrary Optical Pulse Using Dual-Comb Spectroscopy, *Phys. Rev. Appl.* **14**, 014061 (2020).
- [16] J. H. Huh, Z. Chen, E. Vicentini, T. W. Hänsch, and N. Picqué, Time-resolved dual-comb spectroscopy with a single electro-optic modulator, *Opt. Lett.* **46**, 3957 (2021).
- [17] A. J. Fleisher, B. J. Bjork, T. Q. Bui, K. C. Cossel, M. Okumura, and J. Ye, Mid-infrared time-resolved frequency comb spectroscopy of transient free radicals, *J. Phys. Chem. Lett.* **5**, 2241 (2014).
- [18] N. Hoghooghi, R. K. Cole, and G. B. Rieker, 11- μs time-resolved, continuous dual-comb spectroscopy with spectrally filtered mode-locked frequency combs, *Appl. Phys. B* **127**, 17 (2021).
- [19] B. Bernhardt, A. Ozawa, P. Jacquet, M. Jacquy, Y. Kobayashi, T. Udem, R. Holzwarth, G. Guelachvili, T. W. Hänsch, and N. Picque, Cavity-enhanced dual-comb spectroscopy, *Nat. Photonics* **4**, 55 (2010).
- [20] Y. Zhang, R. R. D. Weeks, C. Lecaplain, S. S. Harilal, J. Yeak, M. C. Phillips, and R. J. Jones, Burst-mode dual-comb spectroscopy, *Opt. Lett.* **46**, 860 (2021).
- [21] A. Asahara and K. Minoshima, Development of ultrafast time-resolved dual-comb spectroscopy, *APL Photonics* **2**, 041301 (2017).
- [22] J. Kim, J. Jeon, T. H. Yoon, and M. Cho, Two-dimensional electronic spectroscopy of bacteriochlorophyll *a* with synchronized dual mode-locked lasers, *Nat. Commun.* **11**, 6029 (2020).
- [23] B. Lomsadze, B. C. Smith, and S. T. Cundiff, Tri-comb spectroscopy, *Nat. Photonics* **12**, 676 (2018).
- [24] J. Kim, B. Cho, T. H. Yoon, and M. Cho, Dual-frequency comb transient absorption: Broad dynamic range measurement of femtosecond to nanosecond relaxation processes, *J. Phys. Chem. Lett.* **9**, 1866 (2018).
- [25] See Supplemental Material at <http://link.aps.org/supplemental/10.1103/PhysRevResearch.5.033158> for detailed theoretical calculation and simulation result for the modulated dual-comb spectroscopy method.
- [26] S. Ghosh and G. Eisenstein, Highly coherent hybrid dual-comb spectrometer, *Opt. Express* **31**, 25093 (2023).
- [27] D. Felinto, C. Bosco, L. Acioli, and S. Vianna, Coherent accumulation in two-level atoms excited by a train of ultrashort pulses, *Opt. Commun.* **215**, 69 (2003).
- [28] A. Marian, M. C. Stowe, J. R. Lawall, D. Felinto, and J. Ye, United time-frequency spectroscopy for dynamics and global structure, *Science* **306**, 2063 (2004).
- [29] B. Huber, T. Baluktian, M. Schlagmüller, A. Kölle, H. Kübler, R. Löw, and T. Pfau, GHz Rabi Flopping to Rydberg States in Hot Atomic Vapor Cells, *Phys. Rev. Lett.* **107**, 243001 (2011).
- [30] E. A. Rotberg, B. Barrett, S. Beattie, S. Chudasama, M. Weel, I. Chan, and A. Kumarakrishnan, Measurement of excited-state lifetime using two-pulse photon echoes in rubidium vapor, *J. Opt. Soc. Am. B* **24**, 671 (2007).
- [31] D. Steck, Rubidium 87 D line data, <https://steck.us/alkalidata> (2003).
- [32] D. Steck, Rubidium 85 D line data, <https://steck.us/alkalidata> (2003).
- [33] S. Krämer, D. Plankensteiner, L. Ostermann, and H. Ritsch, QuantumOptics.jl: A Julia framework for simulating open quantum systems, *Comput. Phys. Commun.* **227**, 109 (2018).

- [34] A. Dutt, C. Joshi, X. Ji, J. Cardenas, Y. Okawachi, K. Luke, A. L. Gaeta, and M. Lipson, On-chip dual-comb source for spectroscopy, *Sci. Adv.* **4**, e1701858 (2018).
- [35] B. Lomsadze and S. T. Cundiff, Multi-heterodyne two dimensional coherent spectroscopy using frequency combs., *Sci. Rep.* **7**, 14018 (2017).
- [36] A. Balocchi, Q. H. Duong, P. Renucci, B. L. Liu, C. Fontaine, T. Amand, D. Lagarde, and X. Marie, Full Electrical Control of the Electron Spin Relaxation in GaAs Quantum Wells, *Phys. Rev. Lett.* **107**, 136604 (2011).
- [37] A. V. Trifonov, E. S. Khramtsov, K. V. Kavokin, I. V. Ignatiev, A. V. Kavokin, Y. P. Efimov, S. A. Eliseev, P. Y. Shapochkin, and M. Bayer, Nanosecond Spin Coherence Time of Nonradiative Excitons in GaAs/AlGaAs Quantum Wells, *Phys. Rev. Lett.* **122**, 147401 (2019).